Impact of watershed topography on hyporheic exchange

Impact of watershed topography on hyporheic exchange

Alice Caruso*, Luca Ridolfi, Fulvio Boano

Department of Environment, Land, and Infrastructure Engineering, Politecnico di Torino, Torino, Italy

Abstract

Among the interactions between surface water bodies and aquifers, hyporheic exchange has been recognized as a key process for nutrient cycling and contaminant transport. Even though hyporheic exchange is strongly controlled by groundwater discharge, our understanding of the impact of the regional groundwater flow on hyporheic fluxes is still limited because of the complexity arising from the multiscale nature of these interactions. In this work, we investigate the role of watershed topography on river-aquifer interactions by way of a semi-analytical model, in which the landscape topography is used to approximate the groundwater head distribution. The analysis of a case study shows how the complex topographic structure is alone responsible of a substantial spatial variability of the aquifer-river exchange. Groundwater upwelling along the river corridor is estimated and its influence on the hyporheic zone is discussed. In particular, the fragmentation of the hyporeic corridor induced by groundwater discharge at basin scale is highlighted.

Keywords: SW-GW interactions; river; aquifer; hyporheic exchange; topography; basin scale

1. Introduction

Riverine and groundwater systems are vital compartments for human activities (e.g., agriculture, energy production, navigation), represent important

*Corresponding author
Email address: alice.caruso@polito.it (Alice Caruso)

environments for many ecological and biogeochemical processes, and are essential habitats for several plant and animal species [1, 2, 3, 4]. Therefore, the protection of these systems is an essential element of water resources management. Aquifers and rivers were traditionally studied as separate components of the hydrological system in most ecological research [2, 5], mainly because their physical and chemical characteristics are completely different. However, in the recent decades much attention has been paid to the interactions between surface water and groundwater [6, 3], widely recognising the strong connectivity between rivers and aquifers [7]. To date, many efforts have been made to elucidate the basic physical drivers of groundwater-surface water exchange and its connections with chemical and ecological processes [2, 8, 9].

The hydrodynamic and biogeochemical interactions between surface water and groundwater ~~are characterised by~~ **occur across** a wide range of spatial and temporal scales, which interact and determine a complex system where smaller flow cells (i.e., circulation structures) are nested inside larger flow cells [10, 11, 12]. These different scales reflect the existence of multiple spatial scales characterising landscape and river morphology (from the scale of a single geomorphological unit to **that of** the regional-watershed ~~scale~~), which drive the water movement within the catchment. On the whole, river-aquifer interactions exercise a strong influence on the chemistry and the quality of both surface water and groundwater because the river-sediment interface hosts an intense biogeochemical activity, which affects nutrient cycling (e.g, organic carbon, nitrate and phosphate) [8, 13, 14, 15, 16] and contributes to the natural attenuation or removal of pollutants [17, 18, 19, 20].

A crucial zone where the connection between rivers and aquifers occurs is the hyporheic zone, located in the sediments beneath and adjacent to the river and representing a dynamic ecotone where surface water and groundwater mix [5]. As reported in [12], 'hyporheic flow is commonly distinguished from groundwater flowing near rivers by its bidirectional nature, i.e., hyporheic flow is exchanged back and forth across the streambed interface whereas groundwater recharge or discharge is considered to travel unidirectionally over much longer distances'.

Water exchanges through the streambed are mainly induced by variations in bed topography, permeability and hydrological conditions [21]. Hyporheic pathways reach shallow depths (centimeters or decimeters) if developed beneath small bedforms whereas they infiltrate up to several tens, hundreds, or even thousands of meters when drivers are larger geomorphological features [12]. Laterally, the hyporheic mixing can be limited in small rivers confined by hillslopes but may be extend into the riparian zone, including the wider floodplain and enhancing the formation of a vast habitat suitable for many microbial communities [22, 23, 24]. The spatial variability of hyporheic zone reflects on hyporheic residence times (i.e., the amount of time that river water ~~is~~ **spends** in contact with the groundwater environment before re-emerging into the river), which range from seconds to tens of years and impact hyporheic biogeochemical patterns [12, 25].

The multiple scales at which hyporheic exchange is commonly observed are small, however, if compared with the regional-watershed scales of groundwater fluxes within the aquifers. It is useful to distinguish the small-scale hyporheic fluxes from the interactions induced by large-scale hydraulic head gradients in order to understand how these two different types of river-groundwater interactions affect each other. In fact, the exchange of water and solutes at the small scale typical of hyporheic fluxes is controlled and influenced by groundwater discharge into the river network and, *vice versa*, by the recharge of the aquifer by rivers at large scale. One of the most emblematic situations on which hyporheic and regional flows interact occurs when the river is in gaining conditions, i.e., it is fed by the aquifer. In this situation, the underlying groundwater flow system obstructs the penetration of stream water into the sediments, limiting the extent of the hyporheic zone and the magnitude of hyporheic flow paths [26, 27, 28, 29]. In order to analyse the structure of the hyporheic processes embedded within larger groundwater systems is therefore necessary to describe how the flow originating from the complex surrounding aquifer impacts exchange flux in the hyporheic corridor [30]. Understanding the role of large-scale hydraulic gradients on hyporheic exchange is important for the ~~health~~ **qualitative assessment** of the fluvial ecosystem because of the

implications for river contamination by nutrient and metal and for the biogeochemical and ecological processes occurring along the river corridor [31, 32]. There exist several numerical and field-based studies aimed to advance the understanding of the hydrogeological behaviour of a watershed, which ~~assess~~ **analyse some specific aspects of** groundwater-surface water interaction at large scale ~~analysing some specific aspects~~ (e.g., hydrological stresses, aquifer heterogeneity, etc.). However, the role of the hyporheic zone in this interaction is not here examined in detail [33, 34, 35, 36, 37]. Conversely, some modelling and experimental approaches were developed to specifically investigate the impact of large-scale river-aquifer interactions on the main properties of local exchange at various scales [28, 29, 31, 38].

The influence of groundwater upwelling on bedform-induced hyporheic exchange was investigated by Boano et al. [27, 28], who developed a general simplified mathematical model demonstrating how large-scale exchanges modify the shape and travel time of hyporheic pathways. ~~At the small-scale of river bedforms also~~ Laboratory studies [29] ~~were~~ performed **at the small scale of river bedforms**, ~~which assessed~~ **showing** that increasing losing and gaining stream flow conditions reduce hyporheic fluxes, for a simple case of interaction with small geomorphological structures. Other analyses were conducted at larger scales. Trauth et al. [38, 32] showed by way of a 3D numerical model (which couples a fluid dynamics code to a groundwater flow model) that reductions of the hyporheic exchange flow rate in a pool-riffle stream were caused by an ambient groundwater system, demonstrating how some biogeochemical reactions (aerobic respiration and denitrification) are influenced by variations of gaining and losing conditions. Cardenas [31] analysed via numerical modelling how sinuosity-driven lateral hyporheic exchange is affected by net gains from and net losses ~~of water~~ to the adjacent aquifer. They showed that the exponential reduction in flux when the river loses or gains is more pronounced in straighter channels than in sinuous channels. Gomez-Velez et al. [39, 40] proposed a multi-scale model that investigates the consequences of hyporheic exchange at the watershed scale. Hyporheic exchange in synthetic river networks was eval-

uated by integrating the fluxes induced by single geomorphological features, obtaining a quantification related to the whole river system. Nevertheless, the influence of the upwelling component of regional groundwater flow was considered in a simplified way. All the mentioned studies have provided some insights into the interactions between hyporheic exchange and groundwater flow at different scales. However, a clear and complete evaluation of how hyporheic fluxes interact with groundwater at the watershed scale (generally 10-1000 km in **linear** extent) and are affected by the landscape structure is still missing [12, 29]. Such an evaluation is fundamental to predict the actual behaviour of hyporheic exchange along the river network and its influence on nutrient cycling.

The present work investigates how the geometrical complexity of the water table at the watershed scale ~~impacts on~~ **affects** the spatial patterns of groundwater inflow fluxes in a river network. These groundwater fluxes in turn influence hyporheic exchange since the size of the hyporheic zone is significantly constrained by the upwelling of groundwater.~~, as previously explained.~~ Therefore, our aim is to provide a deeper understanding of how hyporheic processes are influenced by the ambient groundwater flow, examining the impact of groundwater structure at ~~basin~~ **a large** scale on the hyporheic fluxes. Focusing on catchments in humid regions, we consider a case in which the water table can be **plausibly** assumed ~~as a plausible reproduction~~ **to reproduce** of the topographic surface. Under these conditions, the complexity of the water table structure is a direct consequence of the topography complexity, i.e., the geometrical variations of the ground surface elevation spanning a wide range of spatial scales. Our study shows that the complex geometrical structure of the water table is itself able to entail a strong spatial variability of upwelling groundwater (i.e., groundwater upwards flow) along the river corridor and, consequently, of the confinement effect of the hyporheic zone. A statistical analysis of the spatial correlation of groundwater fluxes confirms the high variability of groundwater discharge to the river network. In addition, **the origin and the transit times of groundwater fluxes, which have important implications for the management of chemicals, are evaluated. Finally,** we assess that both the groundwater

fluxes into the river and the transit times of water pathways through the aquifer ~~are characterised by a probability density function that is well approximated by an exponential tail~~ **show a similar behaviour when the analysis is limited to the only main river or extended to the whole river network**.

2. Methods

2.1. Water table modelling and groundwater flow field

Characterising the groundwater table is fundamental in order to examine the groundwater flow field and the groundwater-surface water connection. Water tables at large (regional to continental) scales can be classified as "topography-controlled" or "recharge-controlled", depending on the degree to which they are influenced by the topography [41, 42]. In this study, we considered the case of a water table that is controlled by the topography and that it can be considered a subdued and smoothed version of the ground surface. This assumption has been employed in the literature in both seminal [10, 43] and recent [11, 44, 45] studies and asserts that the water table is fixed and the patterns of recharge and discharge areas are fixed as well. A different approach to groundwater modelling consists of imposing a recharge rate on the top of the aquifer and specifying the hydraulic head where streams interact with the aquifer; in this case, the water table is not prescribed [34].

This assumption allowed us to ~~assume~~ **consider** a water table derived from the topography, introducing a remarkable advantage as terrain elevation data are characterised by higher accuracy, higher resolution and easy accessibility in comparison to precipitation data [46]. The correctness of considering a water table that closely follows the shape of the ground surface will be tested in section 2.2 for our specific case. An orthogonal reference system was chosen, where x and y define the horizontal plane, while z is the vertical direction (positive upward). Here, $z = 0$ is defined as the lowest point of the water table in the catchment.

In the present study, groundwater flow was analysed under steady-state conditions assuming that the groundwater surface was static and neglecting temporal variations. The basic governing differential equation for steady-state groundwater flow in a homogeneous and isotropic medium is the Laplacian equation given by $\nabla^2 h = 0$, where h is the hydraulic head of the groundwater [47]. In a two-dimensional case**, where the transverse flow component is neglected,** an exact solution of the subsurface flow field was obtained by Tóth [10] considering a sinusoidal **spatial** head distribution applied over a flat bed that represented the top boundary of the aquifer. Therefore, for the case of a flow field subject to a sinusoidal **spatial** pressure variation composed by a single harmonic, the solution of the subsurface flow field is known.

To use the analytical solution, we modelled a domain bounded by two horizontal planes located at $z = 0$ and $z = -D$, where D is the finite depth of the aquifer. As boundary conditions, we considered a flat top surface at depth $z = 0$ where the head distribution is imposed (Dirichlet condition) and a no-flow boundary condition at the depth $z = -D$. Mathematically, these boundary conditions mean that $h(x, y, z = 0) = H(x, y)$ and $\partial h/\partial z|_{z=-D} = 0$, where $H(x, y)$ denotes the phreatic surface. Following the approach adopted in previous works [10, 48, 49], the water table can be decomposed into a sum of harmonics each with different amplitude and frequency. Since the Laplace equation is linear, the overall solution can be calculated as sum of the individual solutions related to the single harmonics. Starting from the simplification adopted in [10, 50] and using the superposition principle applied to Darcy groundwater flow, we adopted the approach proposed by Wörman et al. [49] which extended the two-dimensional solutions [10, 50] to three-dimensional domains and derived an analytical expression to determine surface-groundwater flows in three dimensions for an arbitrary topography, that is decomposed in a Fourier series. To this aim, we employed the codes "Spectop" and "Specvel" developed by Wörman et al. [49] for a spectral analysis of the groundwater table.

The application of the described approach requires a spatial distribution of hydraulic head $H(x, y)$ to be prescribed. Digital elevation models (DEMs)

are commonly used to represent the complexity inherent to a real landscape topography. Using topographic data provided by a DEM, landscape topography can be used as a proxy for the phreatic surface H:

$$H(x,y) = \langle h \rangle + \sum_{j=1}^{N_y} \sum_{i=1}^{N_x} (h_m)_{i,j} \sin(k_{x,i}x) \cos(k_{y,j}y) \tag{1}$$

in which $\langle h \rangle$ is areal mean value of the hydraulic head, N_x and N_y are the numbers of real harmonic functions applied in the x and y directions respectively, $(h_m)_{i,j}$ are the amplitude coefficients, $k_{x,i} = 2\pi/\lambda_{x,i}$ and $k_{y,i} = 2\pi/\lambda_{y,i}$ are the wave number, and $\lambda_{x,i}$ and $\lambda_{y,i}$ are the wavelength of the i-th harmonic in each direction. Hence, the periodicity of the water table was examined using a linear combination of harmonics encompassing a wide range of frequencies [49].

Using the boundary conditions and solving the Laplace equation, the three-dimensional head distribution is given by [49]

$$\begin{aligned} h(x,y,z) = \langle h \rangle + \sum_{j=1}^{N_y} \sum_{i=1}^{N_x} (h_m)_{i,j} \cdot \sin(k_{x,i}x) \cos(k_{y,j}y) \cdot \\ \cdot \frac{\exp\left(\sqrt{k_{x,i}^2 + k_{y,j}^2}\, z\right) + \exp\left(\sqrt{k_{x,i}^2 + k_{y,j}^2}(-2D - z)\right)}{1 + \exp\left(-2\sqrt{k_{x,i}^2 + k_{y,j}^2}\, D\right)} \end{aligned} \tag{2}$$

in which $-D \leq z \leq 0$, i.e., the solution is valid only below the plane where the sinusoidal head is applied. Each term of Eq. (2) represents a partial solution to the groundwater flow field related to a specific spatial scale and the relative contribution of each harmonic to the entire signal is provided by the amplitude of that harmonic.

The unknown variables of a Fourier series are the amplitude (or Fourier) coefficients and they can be determined by a least-square fitting of Eq. (1) to the given topographical dataset. The wave numbers can be selected arbitrarily, provided that they respect the constraints for possible wavelengths (i.e., periodicity equal to the domain size and frequencies smaller than the Nyquist frequency) [46]. To model the phreatic surface, the longest wavelength, λ_{max}, was chosen equal to the mean value of the domain lengths in the x and y directions, as suggested by Wörman [49]. The other wavelength values were calculated as

sub-multiples of the longest one. As a result, the shortest wavelength, λ_{min}, was equal to the longest one divided by the number of wavelengths in each direction, i.e. $\lambda_{min} = \lambda_{max}/N$. In addition, we adopted isotropic harmonic functions so that $N_x = N_y = N$ and $\lambda_{x,i} = \lambda_{y,i} = \lambda_i$.

The analytical solution (2) was applied to evaluate the head distribution and, consequently, the subsurface velocity field over the whole domain as $\mathbf{q} = -K\nabla h$, where $\mathbf{q}$ is the Darcy velocity vector, and K is the hydraulic conductivity. Darcy velocity was divided by the soil porosity to obtain an effective velocity, v, of the water within the pores. Similarly to other works [11, 34], we considered a porous medium, with homogeneous and isotropic geologic conditions. While this assumption is not well representative of the real stratigraphy on an aquifer, our objective is to describe the general structure of river-aquifer interaction focusing on the hydraulic heterogeneity induced by the complexity of the water table shape. The value of hydraulic conductivity was chosen through a calibration procedure. For different values of hydraulic conductivity, the groundwater recharge (determined as the total vertical flux at $z = 0$ over the whole basin) was calculated and compared to the measured areal mean value for recharge. The value of K was changed until a good comparison between modelled and observed recharge was obtained.

2.2. Input data

In this section, the input data used to test the model are introduced, in conjunction with the description of the study area they refer to. The choice of a specific study area is not to be interpreted as a restriction of our analyses and results to a specific region. Rather, it is aimed to assess the impact of a realistic landscape topography on river-aquifer interactions, working with topographic data from a real catchment.

The method was applied on the Borbore catchment (44° 53' N; 8° 12' W), located in the Piedmont region of northwest Italy. The total area of the watershed is 506 km^2. The region has a continental climate, with a mean annual air temperature of $\sim$ 13 °C and mean annual rainfall of 723 mm. The basin is

located in a predominantly rural area, and the distribution of land use is 62.8% agricultural lands, 30.7% forest, 4.1% grasslands, 1.9% residential lands, 0.2% shrub land, 0.2% landfill, and 0.1% uncultivated land. The global data set of monthly irrigated and rainfed crop areas (MIRCA 2000, [51]) shows that the Borbore basin is almost entirely rainfed and the percentage of irrigated area is extremely low. Hence, seepage from irrigation canals is not an important source of recharge to shallow groundwater and has a minimal effect on groundwater levels and boundary conditions [52]. The elevation of the landscape ranges from 114 m to 544 m a.s.l., with a mean value of 232 m a.s.l. The annual average discharge of the Borbore river is about 9 m^3/s, which corresponds to a mean annual runoff of about 560 mm. This value was taken as reference value to calibrate the hydraulic conductivity. Information about the study area is provided by the Regional Agency for the Environmental Protection of Piedmont (ARPA), which confirms the absence of a significant irrigation system.

To represent the topography of the study area, we used a DEM with a resolution of 50 m (l_{pixel}= 50 m). A channel-threshold area method for extracting channel networks from DEMs was used. This method consists of specifying a critical support area that defines the minimum drainage area required to initiate a channel [53]. The base of the aquifer was located at a depth $D = 500$ m under the lowest point of the water table, except where specifically indicated. As mentioned in section 2.1, detailed geological and geomorphological aspects are not here taken into account since the analysis of their influence goes beyond the scope of the present work in order to isolate the impact of the water table geometry. The study area is composed mainly of successions of clays and sands and therefore is characterised by low permeability values, coupled to a relatively high precipitation rate. As discussed below, these hydrogeologic properties are compliant with the characteristics required for a topography-controlled water table assumption since they both contribute to cause a shallow water table.

2.3. ~~*Validation*~~ ***Check*** *of the topography-controlled water table assumption*

The parameters required to evaluate the solution in equation (2) are here selected and the topography-controlled water table assumption is ~~validated~~ **tested** for the specific case. The differentiation of the water table into two types, i.e., topography- or recharge-controlled, depends on the aquifer properties and climate characteristics. Some ~~checks~~ **criteria** are suggested in literature to ~~verify~~ **check** if the shape of the water table can be reasonably approximated by landscape topography. Haitjema and Mitchell-Bruker [41] proposed a dimensionless criterion to distinguish under what circumstances groundwater flow is controlled by landscape topography or when it is recharged-controlled. The former situation occurs in humid climates or regions with low topographic relief, where the recharge rate (precipitation) is sufficiently high relative to the infiltration capacity of the ground. In these areas, the groundwater table closely follows the topography. Conversely, in dry climates or regions with high relief, groundwater systems are characterized by deep groundwater tables and there is essentially no correlation between the shapes of the topography and of the water table.

First, we applied Haitjema's criterion [41] to evaluate the soundness of the hypothesis of topography-controlled water table in the study domain. This criterion is based on the evaluation of the following ratio

$$\frac{\Delta h}{d} \simeq \frac{RL^2}{8KDd} \tag{3}$$

in which Δh is the maximum ground water mounding (i.e., the maximum difference in elevation of the water table), d is the maximum terrain rise, R is the recharge rate, and L is the distance between hydrological boundaries. If the ratio $\Delta h/d$ is less than 1, the groundwater circulation can be classified as recharged-controlled; if it is equal to or greater than 1 then the phreatic surface is topography-controlled.

The previous criterion evaluates the ~~validity~~ **correctness** of the hypothesis of topography-controlled water table on the basis of landscape and climate properties averaged over the whole basin. When the water table is modelled as the sum of many harmonics, a more local perspective can be formulated to

choose an appropriate number of wavelengths that takes into account that the groundwater surface undulation is certainly smoother and damped with respect to the landscape topography [50, 54]. Therefore, the number of wavelengths used in the Fourier series must be chosen in order to obtain a water table that is plausible and does not induce high-frequency oscillations which cannot exist in the real water table. The local elevation of the water table is governed by the balance between areal recharge and water flows, and this balance is governed by the following Poisson-like differential equation

$$\nabla^2 H^2 = 2R/K. \tag{4}$$

The Laplacian of H^2 can be numerically calculated for each raster pixel of the groundwater table and compared with the threshold value $2R/K$. If the condition $\nabla^2 H^2/(2R/K) \leq 1$, is satisfied, the water table follows the topography at that point and the assumption is valid. As discussed below, values slightly higher than unity will also be accepted provided they only occur in small parts of the catchment. Following this criterion, the phreatic surface was modelled by Eq. (1) using different numbers of harmonics N. Specifically, we started with a detailed description of the water table using a large number of harmonics, and we gradually eliminated some harmonics until Eq. (4) was verified for a large part of the points of the considered domain. It was observed that the area where the condition (4) was satisfied increased when an even lower number of harmonics was used to model the phreatic surface. On the other hand, a low number of harmonics was insufficient to reproduce a plausible configuration of the water table and, consequently, of the river network. Therefore, a good compromise between these conflicting instances was searched, **choosing a number of harmonics which respects both the requirements satisfactorily** .

On the basis of the above considerations, we selected a number $N = 23$ (N^2=529 terms) of harmonics in each direction to use in the spectral solution given by Eq. (1). The condition $\nabla^2 H^2/(2R/K) \leq 1$ was rigorously satisfied for about 55% of the domain points. In addition, about 95% of the domain points satisfied the condition $\nabla^2 H^2/(2R/K) \leq 3$ and the whole study domain satisfied

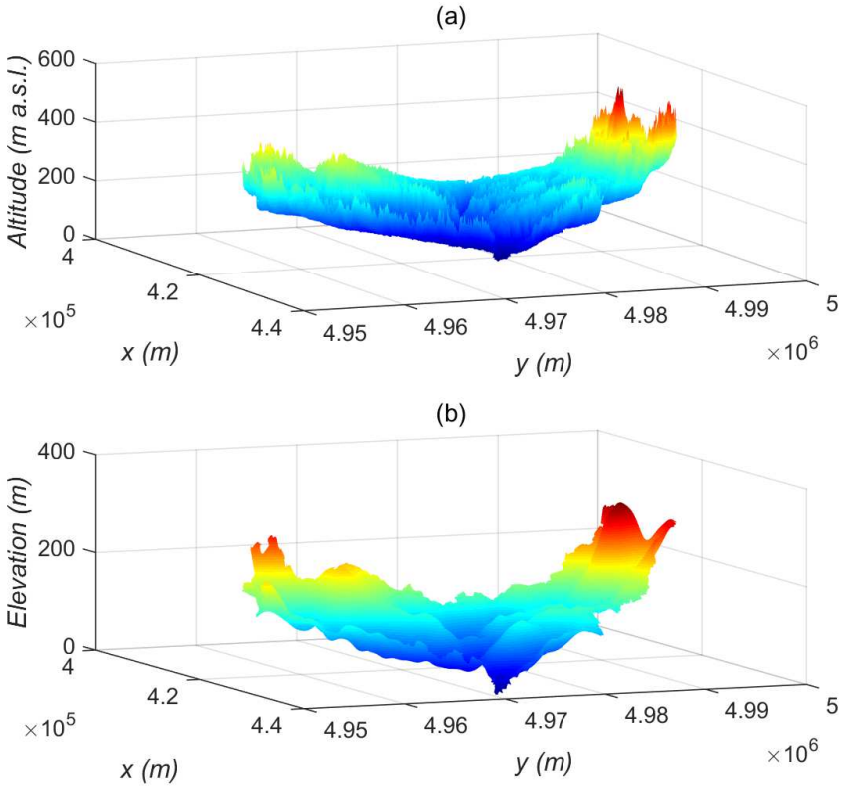

Figure 1: (a) Landscape topography of the study domain according to the digital elevation model (DEM) with resolution 50x50 m. The coordinate system is WGS84/UTM. (b) Representation of the water table obtained by the spectral solution using a number of harmonics $N = 23$ in x- and y- direction. The elevation values are defined with respect to the plane $z = 0$ passing through the lowest point of the water table. Warmer colors indicate higher elevations.

the condition $\nabla^2 H^2/(2R/K) \leq 5$. The application of Eq.(4) at the scale of a single pixel (50 m) allowed us to eliminate steep local hydraulic gradients that are physically unrealistic. Hence, the chosen number of harmonics assured an appropriate modelling of the water table, with a good compromise between the absence of excessive undulations of the water table and the accuracy of the river network. The DEM of the study area and the water table obtained by the spectral representation are shown in Fig. 1. The wavelengths of the phreatic surface range from λ_{min}=1.55 km to λ_{max}=35.5 km.

For the chosen value of N, the calibration procedure explained in section 2.1 has led to a homogeneous hydraulic conductivity of $3.2{\cdot}10^{-6}$ m/s. A value of porosity $n = 0.3$ which is consistent with the prevalent lithology (clay and sand, [55]) was set. Assuming L equal to the characteristic length of the study domain, the ratio $\nabla h/d$ in Eq. (3) is about 4, well above the unitary threshold. Therefore, according to the criterion stated by Haitjema and Mitchell-Bruker, the groundwater circulation in the study domain can be classified as topography-controlled.

2.4. Evaluation of exchange fluxes and groundwater pathway transit times

Once the water table was defined, the groundwater flow field was calculated over the whole domain as explained in section 2.1. The evaluation of the groundwater flow field allowed us to identify discharge and recharge areas in the study basin. Recharge zones are areas where the aquifer is fed by surface water from precipitation or rivers (vertical component of Darcy velocity $q_z < 0$). Conversely, discharge zones are areas where groundwater leaves the aquifer ($q_z > 0$), establishing effluent conditions and contributing to surface water flow. The distribution of recharge and discharge areas is strictly correlated to the configuration of the water table and significantly influences the structure of groundwater circulation [10, 56].

The identification of the groundwater discharge areas requires some attention as the method overestimates the width of the upward groundwater flow zones around the river network (as it is shown later in 3.1). The reason is the lack of

a specific boundary condition imposing the level of the phreatic surface equal to the river head where a river is present. To take into account that some trajectories ending near the river ~~would~~ **could** actually feed the river either as runoff over hillslopes or as direct groundwater flow, we considered a strip of extension B located around and along the river. **When the width of the strip corresponds to the river cell size (i.e., $B = 50$ m), the only trajectories arriving to the river cells are considered.** The discharge of each raster cell (pixel) belonging to this strip was calculated as $Q_i = q_{z,i} \cdot A_{pixel}$, where $q_{z,i}$ is the **Darcy** vertical velocity of the i-th cell and $A_{pixel} = l^2_{pixel}$, and Q_i was attributed to the closest river cell. To quantitatively evaluate the exchange fluxes between the aquifer and the main river, the total groundwater discharge related to each river cell was obtained by the algebraic sum of discharge to the river cells as $Q = \sum Q_i$, where the summation is extended to all cells within the delimited strip of width B. Following this criterion, ~~exchange fluxes between surface and subsurface water were~~ **groundwater discharge to the main river was** quantitatively evaluated in terms of volumetric flow rate of exchanged water for each river cell. **The cumulative flux per unit channel width defined as $f_z = \int_0^L q_z dl$, where L is the river length, was obtained integrating the value of the vertical velocity beneath the riverbed along the channel. This quantity gives an indication of the overall behaviour of the river (i.e, gaining or losing depending on the positive or negative sign of f_z).**

In order to quantify the impact of regional groundwater discharge on hyporheic exchange at smaller scales, the groundwater velocity was first estimated along the river corridor. Then, focusing on predicted hyporheic fluxes induced by bedforms [50], it was possible to evaluate the reduction of the size of hyporheic zone caused by groundwater upwelling through the relationship proposed by Boano et al. (2008) [27]

$$z_H = \frac{1}{k_{dune}} \log\left(\frac{q_z}{u_0}\right), \tag{5}$$

where z_H indicates the hyporheic zone depth, $u_0 = k_{dune} K h_0$ is a typical veloc-

ity scale for the hyporheic flow, $k_{dune} = 2\pi/l_{dune}$ is the bedform wavenumber, l_{dune} is the bedform wavelength, K is the streambed hydraulic conductivity, and h_0 is the amplitude of the hydraulic head profile determined by the presence of bedforms. This head difference is commonly evaluated as [50]

$$h_0 = 0.28\frac{U^2}{2g}\left(\frac{h_{dune}/d}{0.34}\right)^m, \tag{6}$$

where U is the mean stream velocity, h_{dune} is the bedform height, d is the stream depth, g is the gravity acceleration, and m is an exponent equal to 3/8 if $H/d < 0.34$ and 3/2 otherwise. The bedform geometry can be correlated to the flow and bed characteristics through the relations proposed by Julien and Klaassen [57] given as

$$h_{dune} = \eta d\left(\frac{D_{50}}{d}\right)^{0.3}, \quad l_{dune} = \eta\xi d, \tag{7a, b}$$

with d and D_{50} the stream depth and the median sediment diameter of the erodible bed, respectively**, and η and ξ empirical coefficients. The average values of these coefficients are equal to $\bar{\eta} = 2.5$ and $\bar{\xi} = 2.5$.** Moreover, the hyporheic exchange flux per unit bed area was evaluated following the theory proposed by Boano et al.[28] as

$$q_H = q_{H,0}\sqrt{1 - \left(\frac{q_z}{u_0}\right)^2} + \frac{q_z}{\pi}\arcsin\left(\frac{q_z}{u_0}\right) - \frac{q_z}{2}, \tag{8}$$

with $q_{H,0} = u_o/\pi$ the hyporheic exchange flux in neutral conditions [50].

The spatial variability of groundwater upwelling along the river can be inferred from the autocorrelation function of the vertical velocity, ρ_{q_z}. Low values of the autocorrelation function indicate that values of ρ_{q_z} at points located at a given distance are not statistically correlated between themselves (generally it is assumed that a value $|\rho| < 0.2$ indicates an absence of correlation). In order to describe the correlation by varying the level of detail of the water table representation, we chose different values of the number of harmonics N. For each value of N, the value of hydraulic conductivity was conveniently calibrated (as illustrated in section 2.1) and the value of λ_{min} was modified. As previously

explained, λ_{min} is a function of the number of harmonics, N, used to model the phreatic surface and it becomes smaller as the number of harmonics increases.

In order to assess the origin of the groundwater discharging to the river and the time spent in the aquifer, we calculated the groundwater flow trajectories ~~in the aquifer were evaluated~~ by a particle tracking routine [58, 49]. **Different infiltration areas in the basin can entail different physicochemical characteristics because of the effect of land-use type on soil properties. Moreover, longer flow paths and longer contact time with subsurface materials may influence the chemical characteristics of the receiving surface water.** To identify inflow patterns of groundwater to the river, a single particle was placed at the $z = 0$ plane in each discharge cell (which represents the arrival cell for a pathway that feeds the river) within the considered area. The flow field was then reversed to track the streamline backwards. Therefore, the water particle positions were tracked along flow pathways and the location of groundwater discharge along the river network was determined. Finally, we evaluated the groundwater circulation time, i.e. the time spent by a water parcel from its entrance into the soil to its discharge into a surface water body. The transit time T_i of each i-th trajectory was used to obtain the pathway transit time distribution. **The modelled travel times are somewhat underestimated since the distance between the top of the domain and the water table is neglected. However, this underestimation is only relevant for short pathways, while it is negligible for the long times which characterise the tail of the probability density function.**

In order to present results in dimensionless form and obtain their generalisation, we identified the characteristic scales (time scale T_0 and velocity scale q_0) of groundwater flow within the watershed and introduced a suitable normalisation. According to [50] and [59], the dimensionless travel time $\hat{T}_i$ of each flowpath can be expressed as

$$\hat{T}_i = \frac{T_i}{\frac{2\pi}{\lambda_{max}} \cdot \frac{K}{n} \cdot \frac{d}{D} \cdot \tanh\left(\frac{2\pi D}{\lambda_{max}}\right)} = \frac{T_i}{T_0} \tag{9}$$

where λ_{max} and d are the maximum wavelength and the maximum difference in elevation of the water table, respectively, and T_i is the dimensional residence time relative to a trajectory starting from a generic cell. Similarly, the dimensionless Darcy velocity $\hat{q}$ can be evaluated as

$$\hat{q} = \frac{q}{\frac{\lambda_{max}}{2\pi} \cdot \frac{1}{K\Delta} \cdot \tanh^{-1}\left(\frac{2\pi D}{\lambda_{max}}\right)} = \frac{q}{q_0}. \tag{10}$$

Finally, the normalised groundwater discharge $\hat{Q}$ is obtained as

$$\hat{Q} = \frac{Q}{q_0 \cdot A_0}, \tag{11}$$

where Q is the dimensional groundwater discharge and $A_0 = B \cdot l_{pixel}$.

3. Results and Discussion

3.1. Flow field and exchange fluxes

Once the water table is modelled the hydraulic head in each point of the domain is known. Therefore, flow velocity and direction at any depth and the overlying recharge can be completely determined by the equation $\mathbf{q} = -K\nabla h$. According to the direction of water flow, it is possible to distinguish between inflow conditions (negative vertical velocity, $q_z < 0$), where surface water contributes to subsurface flow, and effluent conditions (positive vertical velocity, $q_z > 0$), where groundwater drains into the river. Figure 2 shows the spatial distribution of recharge and discharge zones in conjunction with the values of vertical velocity in each point of the domain. ~~It can be observed that the discharge area configuration in the considered catchment and with reference to an average annual situation follows quite well the structure of the river network.~~ **For the steady state condition (i.e., average annual condition), it can be observed that the configuration of the discharge area agrees quite well with the structure of the river network.** The spatial succession of recharge and discharge areas across a valley is due to the presence of flow systems at different scales and entails that water at close locations may have different origins and, consequently, different chemical properties [10].

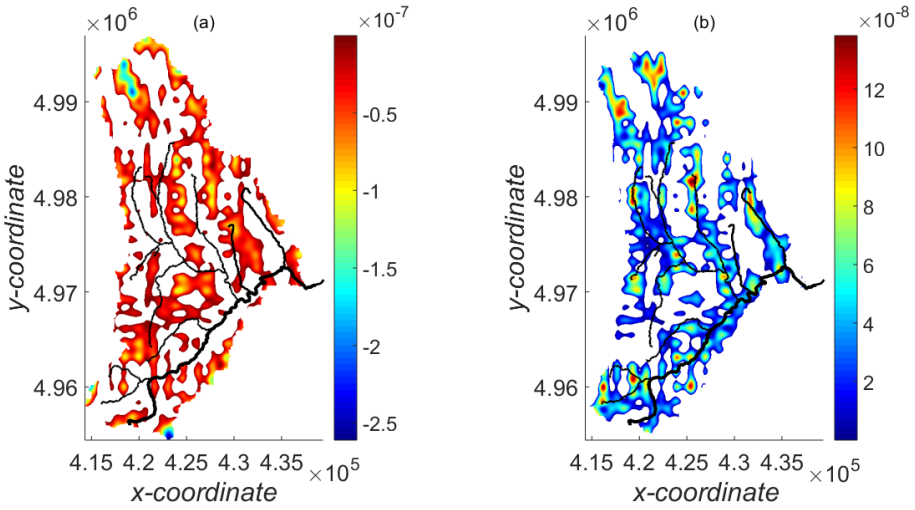

Figure 2: Spatial distribution of recharge areas (a) and discharge areas (b) in the Borbore basin. The colour scale indicates the values of vertical velocity [m/s] of groundwater. The river network is represented: the thicker line indicates the Borbore river, the thinner lines indicate its tributaries.

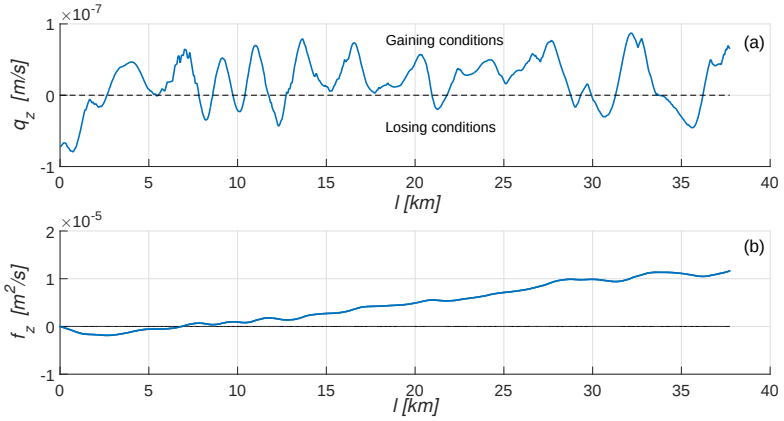

Figure 3: Vertical velocity of groundwater discharge q_z [m/s] (a) and cumulative flux for unit width f_z [m^2/s] (b) as a function of the dimensional downstream distance l along the main river **for** $B = 50$ **m**. Positive and negative values of vertical velocity indicate river gaining and losing conditions, respectively.

The value of the vertical component of the groundwater velocity beneath the river bed indicates whether the river is gaining or losing. **We considered a groundwater discharge area of width equal to the river cell size (i.e., $B = 50$ m) in order to evaluate the overall behaviour of the river and the confining effect of groundwater discharge on hyporheic exchange.** This **velocity** value is represented in Fig. 3a for the main river as a function of the dimensional downstream distance along the channel, l. Positive values represent water gaining river conditions and negative values represent losing river conditions. It should be noticed that water gains and losses are here estimated at the scale of hundreds of meters since the aim is assessing how the hyporheic fluxes are impacted by groundwater upwelling at basin scale. Therefore, Fig. 3 does not consider the water exchange induced by river topography at a smaller scale, i.e., morphological units (such as bars, meanders, step-pools sequences, etc.), which also can affect the patterns of exchange flow and, consequently, the transport of nutrients and contaminants. As it is possible to observe in Fig. 3b, which depicts the cumulative flux per unit channel width f_z **defined in section 2.4,** ~~along the river $f_z = \int_0^x q_z dl$~~ the net surface-subsurface exchange flux is positive, i.e., most of the river is gaining. However, there are also some reaches where the river recharges the aquifer (i.e., losing flow conditions).

The confinement effect of groundwater discharge on hyporheic exchange is exemplified for two representative river reaches (in upstream and downstream areas of the basin) under gaining conditions. For these reaches, the vertical extent of the hyporheic zone (see Fig. 4) and the rate of the hyporheic flux (see Fig. 5) were evaluated through the relationships (5) and (8), respectively. The stream characteristics of the reaches were evaluated on the basis of data provided by ARPA, resulting in **medium characteristic values given by** $(\bar{d}, \bar{U})$=(0.45 m, 1.10 m/s) for the upstream reach and $(\bar{d}, \bar{U})$=(0.95 m, 0.95 m/s) for the downstream reach. The bedform geometry was calculated using Eq. (7) obtaining $(\bar{h}_{dune}, \bar{l}_{dune})$=(0.1 m, 2.80 m) for the upstream reach and $(\bar{h}_{dune}, \bar{l}_{dune})$=(0.15 m, 5.95 m) for the downstream reach. The calibrated hydraulic conductivity value was used, and the median grain size $D_{50} = 10^{-4}$ m,

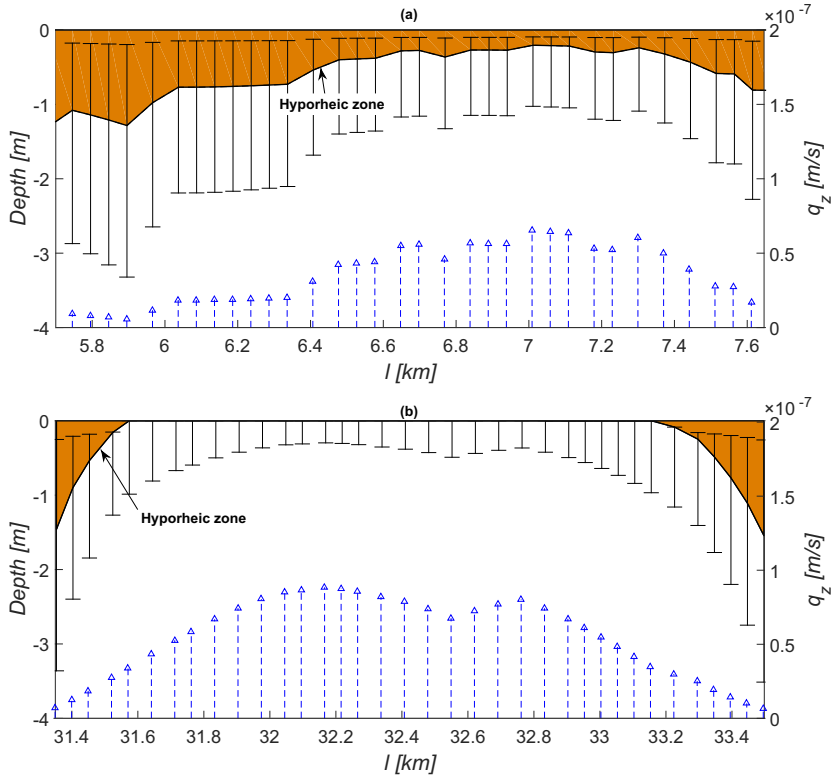

Figure 4: Hyporheic zone depth (left vertical axis) for (a) an upstream and (b) a downstream gaining reach **for average hydraulic and morphodynamic parameters. Error bars represent maximum variations induced by the considered ranges of** U, d, h_{dune}, **and** l_{dune} **is marked by the bars.** The arrows indicate the intensity of groundwater upwelling **for** $B = 50$ **m** (right vertical axis).

which corresponds to a fine sand, was assumed. The hyporhic zone depth ranges from 0.20 m to 1.30 m in the upstream reach and from 0 m to 1.5 m in the downstream reach. Similarly, the hyporheic fluxes range from $7 \cdot 10^{-9}$ m/s to $3 \cdot 10^{-8}$ m/s in the upstream reach and from $7.4 \cdot 10^{-9}$ m/s to 0 in the downstream reach. ~~Therefore,~~ **Overall**, it can be observed that high upwelling velocities counteract the penetration of the river water in the streambed sediments, reducing the depth (Fig. 4) and the intensity (Fig. 5) of hyporheic exchange and sometimes preventing the development of bedform induced flow. In fact, the flow from the stream to the hyporheic zone is totally suppressed when groundwater ~~discharge~~ **upwelling velocity** is equal or higher than the velocity of the hyporheic flow and this happens in a large part of the downstream reach. Therefore, we can state that the vertical extent and the rate of hyporheic exchange are highly variable since they reflect the variability of the groundwater upwelling. The amount and depth of solute exchange with the river will consequently be influenced **by the variation in groundwater input**.

In order to make the results more general and representative, we assessed how hyporheic exchange is expected to be influenced by the variability of the hydraulic and morphological features of the stream. Specifically, a variation of $\pm 10\%$ was adopted for the flow parameters (i.e., $d = \bar{d} \pm 10\%$ and $U = \bar{U} \pm 10\%$). Moreover, the dune height defined by Eq. (7a) was varied considering $0.8 < \eta < 8$, as observed in [57]. A range of dune lengths was then calculated imposing a ratio $h_{dune}/l_{dune} = 5 - 10\%$ [60]. In this way $h_{dune} \in$ [0.03 m, 0.31 m] and $l_{dune} \in$ [0.27 m, 6.17 m] were obtain in the downstream reach, while $h_{dune} \in$ [0.04 m, 0.52 m] and $l_{dune} \in$ [0.45 m, 10.41 m] in the downstream reach. The maximum variation of the hyporheic zone depth for the considered parameter ranges is shown by the bars in Fig. 4. High and long dunes increase the hyporheic zone depth. The dune size exerts a stronger influence on hyporheic zone depth than the flow characteristics. Variations of the hydromorphological features also affects the rate of the hyporheic exchange, which is found to be

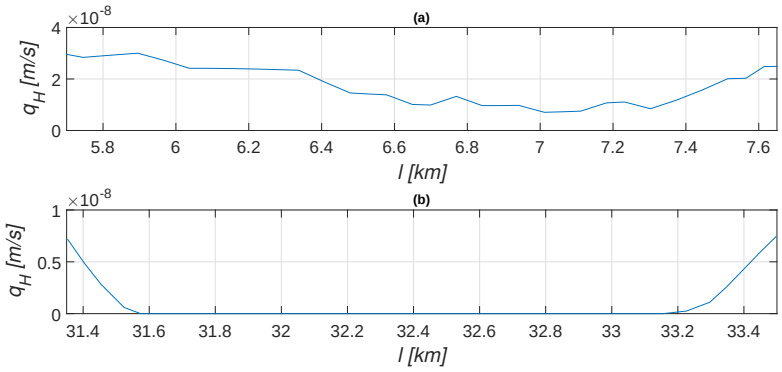

Figure 5: Hyporheic flux per unit bed area in (a) an upstream and (b) a downstream reach in gaining conditions.

highest for the smallest bedforms that correspond to the shallowest hyporheic zones.

~~Figure 6 shows~~ The autocorrelogram of the vertical velocity **shown in Fig.6 provides information about the spatial variability of groundwater discharge. It is** plotted as a function of a normalised downstream distance, $\hat{l} = l/\lambda_{min}$, in order to identify the spatial scale that characterises the variability in exchange fluxes and to obtain a generalized result that is valid regardless of the watershed size. It can be observed that the spatial correlation decreases to small values ($|\rho| < 0.2$) at a dimensionless distance comparable to the unit value (always in the range 0.5-1.5), and it remains low except for some short reaches in which $|\rho|$ is slightly higher than 0.2. Therefore, the typical correlation scale, $\mathcal{C}$, is approximately equal to λ_{min}, i.e., $\mathcal{C} = \mathcal{O}(\lambda_{min})$. This means that the vertical velocities related to river reaches (i.e., pixels) more distant than λ_{min} are statistically uncorrelated. The only correlation could be obtained for $\hat{l} \leq 1$, i.e., for reaches closer than λ_{min}. However, λ_{min} represents the resolution with which the water table is modelled, hence it is not possible to consider results obtained for $l < \lambda_{min}$ ($\hat{l} < 1$) as reliable because the observed correlation is at least partially determined by the periodicity of the smallest harmonic function. This result indicates that the vertical exchange velocity is essentially uncorre-

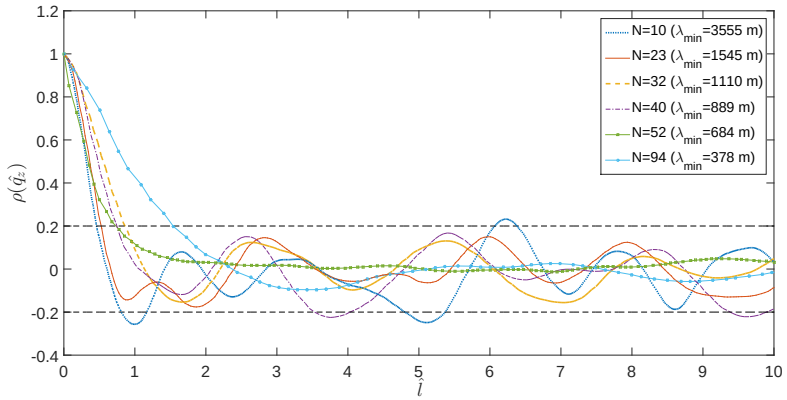

Figure 6: Autocorrelogram of the vertical velocity ρ_{q_z} as a function of the dimensionless downstream distance $\hat{l} = l/\lambda_{min}$ for different values of the number of harmonics N used in the spectral solution (2).

lated along the Borbore river since for $l > \lambda_{min}$ a significant correlation does not exist and for $l < \lambda_{min}$ results are not truly reliable. Introducing more spatial scales and describing in greater detail the water table, the autocorrelation scale of the vertical velocity as a function of the dimensional downstream distance is reduced and more complexities arise in the phreatic surface representation. Hence, the smaller scales lead to less correlation over space and entail a more complex description of the groundwater flow field.

In Fig. 2 (b) we showed that wide upward groundwater flow areas exist, which largely extend around the stream channel. However, considering that this result is at least in part a consequence of the hypothesis of topography controlled water table, as explained in section 2.3, it is reasonable that the actual groundwater discharge is limited to the streambed. Considering ~~two~~ **three** different values of the discharge area width, $B = 50$ **m,** $B = 200$ m and $B = 1000$ m, we evaluated how the spatial pattern of the groundwater discharge into the river varies with the size of this contributing area since the actual width of this strip is uncertain.

Figure 7a shows the groundwater discharge into the main river for the ~~two~~ **three** different discharge areas of width equal to $B = 50$ **m,** $B = 200$ m and

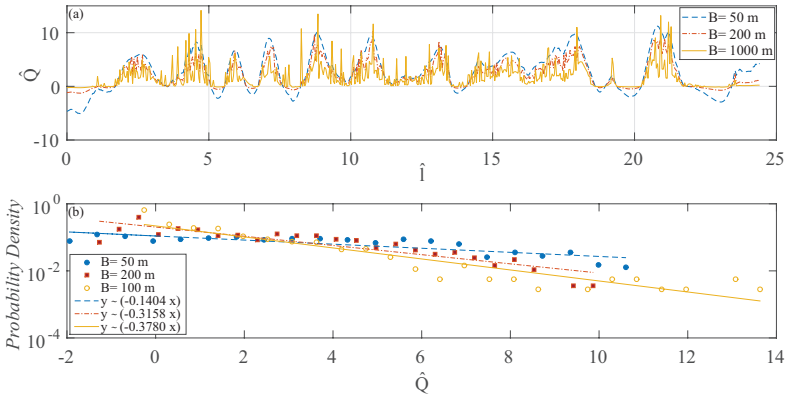

Figure 7: Profile of the dimensionless groundwater discharge, $\hat{Q}$, to the main river (a) and probability density function of the groundwater discharge (b) for ~~two~~ **three** different extension of the area feeding the river.

$B = 1000$ m (i.e., **the only river cell in the first case and** a distance of 100 m and 500 m on each side of the river **in the other two cases**). The figure reveals the presence of a strong spatial variability of the groundwater discharge along the river. This variability is expected to influence the river-hyporheic zone exchange, enhancing the formation of different environmental conditions along the river ecosystem. The spatial distribution of groundwater discharge shows more peaks for the larger width of the contributing area and a smoother behaviour for the narrower band. However, the high degree of irregularity observable in ~~both~~ **all** cases indicates that the exchange between the river and the aquifer can be quite different even among adjacent reaches along the stream. Field and numerical studies frequently found similar high variability in the intensity and also in the direction of exchange fluxes [61, 62]. In our specific case, this strong spatial variability is attributable uniquely to the complex multiscale groundwater flow field induced by watershed topography since other factors (such as heterogeneity of the aquifer geology, river bed morphology, etc.) are not included here. Among the several potential causes of natural variability in a river-aquifer system, the geometrical structure of the water table is therefore able to induce heterogeneity in exchange fluxes along

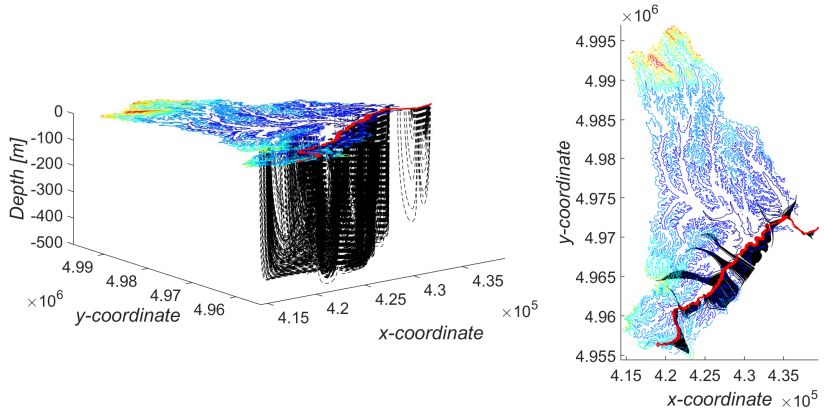

Figure 8: Results from particle tracking simulation in 3D (a) and 2D (b) view. The black lines represent the groundwater pathways that discharge in the main the river.

the river. From this result, it can be inferred that groundwater upwelling acts ~~more or less randomly~~ **quite irregularly** in confining the hyporheic fluxes, as is observable also in Figs. 4 and 5. This implies ~~the lack of a~~ **that there is no** typical scale imposed by groundwater upwelling, i.e., a scale equal or greater than the minimum scale used to model the phreatic surface does not emerge. Consequently, this ~~randomness~~ **heterogeneity** will reflect on the extension of the hyporheic zone and on all processes linked to the hyporheic fluxes (such as chemical reactions, biogeochemical and ecological processes, etc.), which in turn will be not characterised by a typical scale imposed by upwelling.

The probability density function of exchange discharge between the river and the aquifer is represented in Fig. 7b for the ~~two~~ **three** examined cases. It can be observed that the values are well modelled by an exponential tail (straight lines in Fig. 7b, $R^2 = 0.69$ **for** $B = 50$ **m,** $R^2 = 0.79$ for $B = 200$ m and $R^2 = 0.87$ for $B = 1000$ m). Moreover, the ~~two~~ **three** examined cases gives very similar results: this means that the adopted normalisation allows us to eliminate substantially the dependence on the dimensional parameters and to obtain a general result.

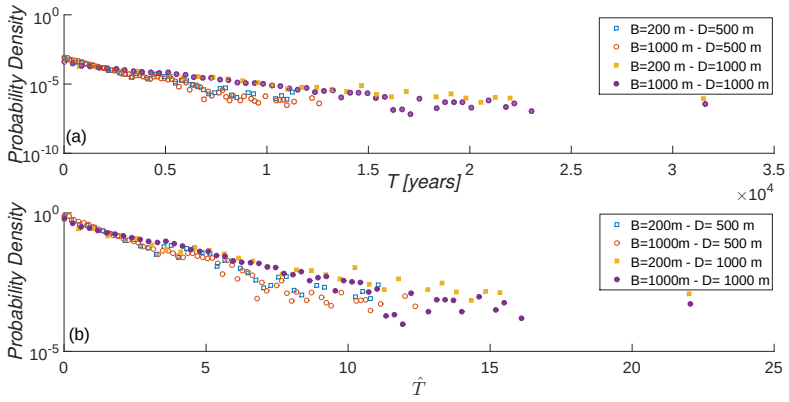

Figure 9: Probability density functions of transit times, calculated using the particle tracking method. Distributions of travel times in dimensional (a) and dimensionless (b) form. The dimensionless time, $\hat{T}$, is defined in (9). Simulations are performed for two different depths of the impermeable layer, $D = 500$ m and $D = 1000$ m, and two different widths of the contributing area, $B = 200$ m and $B = 1000$ m.

3.2. Flow trajectories and residence times

The evaluation of groundwater pathways and transit time distribution is initially limited only to the main river in order to identify the areas of the basin directly feeding the main river by groundwater discharge. The streamlines were calculated for two different values of depth of the impermeable layer, $D = 500$ m and $D = 1000$ m, in order to investigate the influence of this parameter on the transit times. In addition, two different contributing areas of width $B = 200$ m and $B = 1000$ m were considered. Figure 8 shows the groundwater pathways feeding the main river obtained for $D = 500$ m and $B = 200$ m. It can be detected that only part of the whole basin feeds the base flow of the main river (Borbore river). In the represented case, the length of the trajectories ranges from 5 m to 10 km, with a mean value of 2 km. The mean distance reached by the trajectories is 3 km.

The transit time of each trajectory was calculated and the probability density function for each simulation is reported in Fig. 9, in dimensional (Fig. 9a) and dimensionless (Fig. 9b) form. It can be observed that the transit

time distribution follows an exponential decrease ($R^2 = 0.88 - 0.94$), similar to the structure of the discharge distribution. This result is consistent with other works on humid catchments with similar geological settings [34, 63], which show how the exponential behaviour of the transit times distribution is characteristic of groundwater flow at the catchment scale within homogeneous aquifers with uniform recharge. However, other studies [44, 11] found residence time distributions with power-law tails. This difference can be explained considering the aspect ratio of the domain. Specifically, when the aquifer is sufficiently deep ($\tanh(2\pi D/L) \simeq 1$), the influence of the impervious bottom on the flow field is limited, while when the domain is shallow enough so that $\tanh(2\pi D/L) \ll 1$, the influence of the bottom is relevant. In this work, the impermeable bottom layer is relatively shallow in comparison with the longitudinal extension of the study domain, i.e., $D/L \ll 0.02 - 0.03$ from which $\tanh(2\pi D/L) \simeq 0.1 - 0.2$. In particular, the presence of a shallow bottom prevents the presence of the previously long and deep streamlines, which are confined to the shallow parts of the aquifer. This causes shorter trajectories and shorter residence times and leads to the observed exponential tailing, eliminating the very long trajectories that are responsible of a power-law tailing behaviour. As for the discharge Q^*, the results suggest that the adopted normalised scale allows us to obtain a general behaviour since dimensionless curves are similar regardless of the values D and B. The dimensional results show that a deeper aquifer results in longer transit times, while the width B has no relevant effect.

Finally, the analysis of groundwater discharge and water pathways was extended to the whole river network. The simulations were carried out for $B = 200$ m and $D = 500$ m. Fig. 10a represents a comparison of the probability density function of groundwater discharge between the cases in which only the main river and the whole river network are considered. A similar comparison was also implemented for the transit times and is shown in Fig. 10b. It can be observed that the exponential model is preserved and the behaviour is very similar. Therefore, the results can suggest a fractal nature of groundwater-surface water exchange, as discussed in [44].

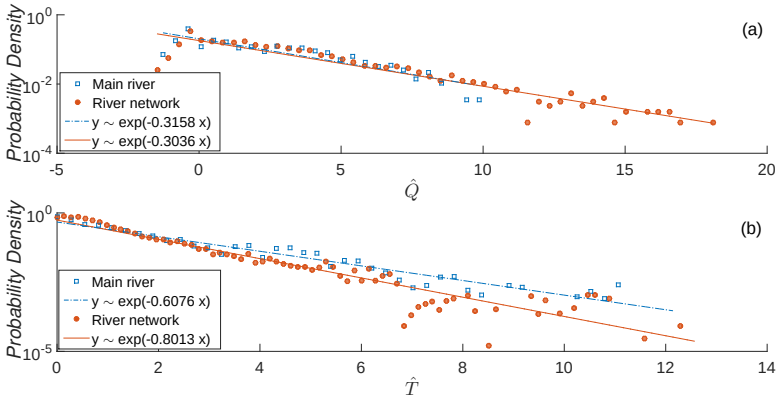

Figure 10: Comparison between groundwater flow results for the main river and the whole river network. Probability density function of groundwater discharge (a) and of travel times (b) are reported in dimensionless form.

4. Conclusions

Landscape topography is among the major factors that control the interaction between surface and subsurface waters, since it represents the dominant driver for groundwater movement at large scales. A study of the role of topographic complexity in controlling river-aquifer exchange has been presented in this work. We have focused on the effects induced by the ground surface structure, considering a simplified system composed by a homogeneous and isotropic aquifer.

The connectivity between the river and the aquifer has many important ecological and environmental effects on the fluvial ecosystem, because it affects the quality and quantity of surface and subsurface water. A crucial point for biogeochemical pathways and nutrient cycling rates is the groundwater-surface water interface, since it controls the flux of groundwater solutes discharging into rivers, and *vice versa*. Studying subsurface-surface water interactions at large scales is useful to identify the zones of a catchment that are more important in determining where groundwater is discharging into the river and where attenuation of groundwater pollutants at the groundwater-surface water interface

might reduce the concentration of pollutants in river water.

The analysis of a simplified real case study has demonstrated how the river-aquifer interaction is influenced by landscape topography, which induces spatial heterogeneity in groundwater discharge to the river. Groundwater discharge exhibits substantial spatial variations induced by the complex structure of the water table, even among adjacent reaches along the river. This result suggests that groundwater upwelling related to a river reach should be modelled as a spatially ~~random~~ **fluctuating** variable when an analysis at smaller scales is implemented. We have observed that a more detailed description of the water table entails a reduction of the spatial correlation scale of exchange fluxes since the representation of the phreatic surface becomes more complex. Overall, a lack of autocorrelation of the vertical exchange velocity along the river is evidenced. An exponential behaviour has been found both for groundwater discharge and transit time distribution.

This study ~~can be intended as a first important step to conceptualise~~ **represents an important step in conceptualising** how the structure of a regional aquifer influences groundwater upwelling, which, in turn, defines and constrains hyporheic exchange (i.e., limits the extent of the hyporheic zone). The strong impact of groundwater discharge at the reach scale on hyporheic fluxes at smaller scales influences the exchange of water and solutes between the river and the hyporheic zone. Therefore, the source of spatial complexity in hyporheic fluxes is not only the geomorphological river complexity but also the topographic structure of the whole basin. The landscape structure substantially affects the groundwater flow field, which plays a key role in defining the depth and the intensity of the hyporheic exchange since it confines and embeds the hyporheic zone. These results represent a complement to existing frameworks to analyse the consequences of hyporheic exchange on water quality and stream ecology at large watershed scales.

The analyses developed to reach the aims of the study are independent of the specific approach used to obtain the water table and could be implemented using more refined (but computationally demanding) numerical methods, obtaining

similar qualitative results, since they are due to the intrinsic complexity of the groundwater table. Future efforts will be certainly devoted to increase the complexity of the system and to verify the impact of factors such as geological variability on the results. It is expected that the inclusion of other factors of natural complexity will further complicate the spatial patterns of exchange fluxes. In fact, other factors could contribute to the strong spatial heterogeneity in fluxes observed in various field studies. Therefore, the main finding regarding the almost random confinement of the hyporheic zone would be confirmed also in a more complex system.

5. Acknowledgements

Authors wish to thank Anders Wörman for providing clarification on the method. Martin S. Andersen and the anonymous reviewers are greatly acknowledge for their valuable suggestions which improved the manuscript.

References

[1] G. P. Malanson, Riparian landscapes, Cambridge University Press, 1993.

[2] M. Brunke, T. Gonser, The ecological significance of exchange processes between rivers and groundwater, Freshwater biology 37 (1) (1997) 1–33. doi:10.1046/j.1365-2427.1997.00143.x.

[3] M. Sophocleous, Interactions between groundwater and surface water: the state of the science, Hydrogeology journal 10 (1) (2002) 52–67. doi:10.1007/s10040-001-0170-8.

[4] M. Hayashi, D. O. Rosenberry, Effects of ground water exchange on the hydrology and ecology of surface water, Groundwater 40 (3) (2002) 309–316.

[5] A. J. Boulton, S. Findlay, P. Marmonier, E. H. Stanley, H. M. Valett, The functional significance of the hyporheic zone in streams and rivers, Annual Review of Ecology and Systematics (1998) 59–81.

[6] J. Stanford, J. Ward, The hyporheic habitat of river ecosystems, Nature Publishing Group, 1988.

[7] K. E. Bencala, R. A. Walters, Simulation of solute transport in a mountain pool-and-riffle stream: A transient storage model, Water Resources Research 19 (3) (1983) 718–724.

[8] N. B. Grimm, S. G. Fisher, Exchange between interstitial and surface water: implications for stream metabolism and nutrient cycling, Hydrobiologia 111 (3) (1984) 219–228.

[9] J. B. Jones, R. M. Holmes, Surface-subsurface interactions in stream ecosystems, Trends in Ecology & Evolution 11 (6) (1996) 239–242.

[10] J. Tóth, A theoretical analysis of groundwater flow in small drainage basins, Journal of Geophysical Research 68 (16) (1963) 4795–4812. doi:10.1029/JZ068i016p04795.

[11] M. B. Cardenas, Potential contribution of topography-driven regional groundwater flow to fractal stream chemistry: Residence time distribution analysis of Tóth flow, Geophysical Research Letters 34 (5) (2007) L05403.

[12] F. Boano, J. W. Harvey, A. Marion, A. I. Packman, R. Revelli, L. Ridolfi, A. Wörman, Hyporheic flow and transport processes: Mechanisms, models, and biogeochemical implications, Reviews of Geophysics 52 (4) (2014) 603–679.

[13] J. W. Harvey, C. C. Fuller, Effect of enhanced manganese oxidation in the hyporheic zone on basin-scale geochemical mass balance, Water Resources Research 34 (4) (1998) 623–636.

[14] T. J. Battin, L. A. Kaplan, S. Findlay, C. S. Hopkinson, E. Marti, A. I. Packman, J. D. Newbold, F. Sabater, Biophysical controls on organic carbon fluxes in fluvial networks, Nature Geoscience 1 (2) (2008) 95–100.

[15] L. Bardini, F. Boano, M. Cardenas, R. Revelli, L. Ridolfi, Nutrient cycling in bedform induced hyporheic zones, Geochimica et Cosmochimica Acta 84 (2012) 47–61.

[16] A. Sawyer, Enhanced removal of groundwater-borne nitrate in heterogeneous aquatic sediments, Geophysical Research Letters 42 (2) (2015) 403–410.

[17] A. R. Hill, Nitrate removal in stream riparian zones, Journal of environmental quality 25 (4) (1996) 743–755.

[18] C. Gandy, J. Smith, A. Jarvis, Attenuation of mining-derived pollutants in the hyporheic zone: A review, Science of the Total Environment 373 (2) (2007) 435–446.

[19] J. Smith, B. W. Surridge, T. Haxton, D. Lerner, Pollutant attenuation at the groundwater–surface water interface: A classification scheme and statistical analysis using national-scale nitrate data, Journal of hydrology 369 (3) (2009) 392–402.

[20] S. B. Grant, K. Stolzenbach, M. Azizian, M. J. Stewardson, F. Boano, L. Bardini, First-order contaminant removal in the hyporheic zone of streams: physical insights from a simple analytical model, Environmental science & technology 48 (19) (2014) 11369–11378.

[21] D. Tonina, J. M. Buffington, Hyporheic exchange in mountain rivers i: Mechanics and environmental effects, Geography Compass 3 (3) (2009) 1063–1086.

[22] J. A. Stanford, J. Ward, An ecosystem perspective of alluvial rivers: connectivity and the hyporheic corridor, Journal of the North American Benthological Society (1993) 48–60.

[23] W. W. Woessner, Stream and fluvial plain ground water interactions: rescaling hydrogeologic thought, Groundwater 38 (3) (2000) 423–429.

[24] J. Stanford, Landscapes and riverscapes, Elsevier: Amsterdam, 2006.

[25] T. Kasahara, S. M. Wondzell, Geomorphic controls on hyporheic exchange flow in mountain streams, Water Resources Research 39 (1) (2003) SBH–3.

[26] G. J. Wroblicky, M. E. Campana, H. M. Valett, C. N. Dahm, Seasonal variation in surface-subsurface water exchange and lateral hyporheic area of two stream-aquifer systems, Water Resources Research 34 (3) (1998) 317–328.

[27] F. Boano, R. Revelli, L. Ridolfi, Reduction of the hyporheic zone volume due to the stream-aquifer interaction, Geophysical Research Letters 35 (9) (2008) L09401.

[28] F. Boano, R. Revelli, L. Ridolfi, Quantifying the impact of groundwater discharge on the surface–subsurface exchange, Hydrological processes 23 (15) (2009) 2108–2116.

[29] A. Fox, F. Boano, S. Arnon, Impact of losing and gaining streamflow conditions on hyporheic exchange fluxes induced by dune-shaped bed forms, Water Resources Research 50 (3) (2014) 1895–1907.

[30] M. B. Cardenas, J. L. Wilson, Exchange across a sediment–water interface with ambient groundwater discharge, Journal of Hydrology 346 (3) (2007) 69–80.

[31] M. B. Cardenas, Stream-aquifer interactions and hyporheic exchange in gaining and losing sinuous streams, Water Resources Research 45 (6) (2009) W06429.

[32] N. Trauth, C. Schmidt, M. Vieweg, U. Maier, J. H. Fleckenstein, Hyporheic transport and biogeochemical reactions in pool-riffle systems under varying ambient groundwater flow conditions, Journal of Geophysical Research: Biogeosciences 119 (5) (2014) 910–928.

[33] S. Krause, A. Bronstert, The impact of groundwater–surface water interactions on the water balance of a mesoscale lowland river catchment in northeastern Germany, Hydrological Processes 21 (2) (2007) 169–184.

[34] P. Goderniaux, P. Davy, E. Bresciani, J.-R. Dreuzy, T. Borgne, Partitioning a regional groundwater flow system into shallow local and deep regional flow compartments, Water Resources Research 49 (4) (2013) 2274–2286. doi:10.1002/wrcr.20186.

[35] S. Bartsch, S. Frei, M. Ruidisch, C. L. Shope, S. Peiffer, B. Kim, J. H. Fleckenstein, River-aquifer exchange fluxes under monsoonal climate conditions, Journal of Hydrology 509 (2014) 601–614.

[36] B. Giambastiani, A. McCallum, M. Andersen, B. Kelly, R. Acworth, Understanding groundwater processes by representing aquifer heterogeneity in the maules creek catchment, namoi valley (new south wales, australia), Hydrogeology Journal 20 (6) (2012) 1027–1044.

[37] A. M. McCallum, M. S. Andersen, B. Giambastiani, B. F. Kelly, R. Ian Acworth, River–aquifer interactions in a semi-arid environment stressed by groundwater abstraction, Hydrological Processes 27 (7) (2013) 1072–1085.

[38] N. Trauth, C. Schmidt, U. Maier, M. Vieweg, J. H. Fleckenstein, Coupled 3-D stream flow and hyporheic flow model under varying stream and ambient groundwater flow conditions in a pool-riffle system, Water Resources Research 49 (9) (2013) 5834–5850.

[39] J. D. Gomez-Velez, J. W. Harvey, A hydrogeomorphic river network model predicts where and why hyporheic exchange is important in large basins, Geophysical Research Letters 41 (18) (2014) 6403–6412.

[40] J. D. Gomez-Velez, J. W. Harvey, M. B. Cardenas, B. Kiel, Denitrification in the mississippi river network controlled by flow through river bedforms, Nature Geoscience 1752 (2015) 0894.

[41] H. M. Haitjema, S. Mitchell-Bruker, Are water tables a subdued replica of the topography?, Ground Water 43 (6) (2005) 781–786. doi:10.1111/j.1745-6584.2005.00090.x.

[42] T. Gleeson, L. Marklund, L. Smith, A. H. Manning, Classifying the water table at regional to continental scales, Geophysical Research Letters 38 (5) (2011) L05401.

[43] D. Ophori, J. Toth, Characterization of ground-water flow by field mapping and numerical simulation, ross creek basin, alberta, canada, Groundwater 27 (2) (1989) 193–201.

[44] A. Wörman, A. I. Packman, L. Marklund, J. W. Harvey, S. H. Stone, Fractal topography and subsurface water flows from fluvial bedforms to the continental shield, Geophysical Research Letters 34 (7) (2007) L07402.

[45] X.-W. Jiang, L. Wan, M. B. Cardenas, S. Ge, X.-S. Wang, Simultaneous rejuvenation and aging of groundwater in basins due to depth-decaying hydraulic conductivity and porosity, Geophysical Research Letters 37 (5) (2010) L05403.

[46] L. Marklund, A. Wörman, The use of spectral analysis-based exact solutions to characterize topography-controlled groundwater flow, Hydrogeology Journal 19 (8) (2011) 1531–1543. doi:10.1007/s10040-011-0768-4.

[47] J. Bear, A.-D. Cheng, Modeling groundwater flow and contaminant transport, Vol. 23, Springer Science & Business Media, 2010.

[48] W. Zijl, Scale aspects of groundwater flow and transport systems, Hydrogeology Journal 7 (1) (1999) 139–150.

[49] A. Wörman, A. I. Packman, L. Marklund, J. W. Harvey, S. H. Stone, Exact three-dimensional spectral solution to surface-groundwater interactions with arbitrary surface topography, Geophysical Research Letters 33 (7) (2006) L07402. doi:10.1029/2006GL025747.

[50] A. H. Elliott, N. H. Brooks, Transfer of nonsorbing solutes to a streambed with bed forms: Theory, Water Resources Research 33 (1) (1997) 123–136.

[51] F. T. Portmann, S. Siebert, P. Döll, MIRCA2000–Global monthly irrigated and rainfed crop areas around the year 2000: A new high-resolution data set for agricultural and hydrological modeling, Global Biogeochemical Cycles 24 (1) (2010) BG1011.

[52] A. Fernald, V. Tidwell, J. Rivera, S. Rodríguez, S. Guldan, C. Steele, C. Ochoa, B. Hurd, M. Ortiz, K. Boykin, et al., Modeling sustainability of water, environment, livelihood, and culture in traditional irrigation communities and their linked watersheds, Sustainability 4 (11) (2012) 2998–3022.

[53] D. R. Montgomery, E. Foufoula-Georgiou, Channel network source representation using digital elevation models, Water Resources Research 29 (12) (1993) 3925–3934.

[54] D. M. Wolock, C. V. Price, Effects of digital elevation model map scale and data resolution, Water Resources Research 30 (11) (1994) 3041–3052.

[55] R. Heath, Basic ground-water hydrology: Us geological survey water-supply paper 2220, 84 p. 1984, Ground-water regions of the United States: US Geological Survey Water-Supply Paper 2242 (1983) 78.

[56] O. Batelaan, F. De Smedt, L. Triest, Regional groundwater discharge: phreatophyte mapping, groundwater modelling and impact analysis of land-use change, Journal of Hydrology 275 (1) (2003) 86–108.

[57] P. Y. Julien, G. J. Klaassen, Sand-dune geometry of large rivers during floods, Journal of Hydraulic Engineering 121 (9) (1995) 657–663.

[58] M. Salehin, A. I. Packman, M. Paradis, Hyporheic exchange with heterogeneous streambeds: Laboratory experiments and modeling, Water Resources Research 40 (11) (2004) W11504.

[59] A. I. Packman, M. Salehin, M. Zaramella, Hyporheic exchange with gravel beds: basic hydrodynamic interactions and bedform-induced advective flows, Journal of Hydraulic Engineering 130 (7) (2004) 647–656.

[60] M. S. Yalin, E. Karahan, Steepness of sedimentary dunes, Journal of the Hydraulics Division 105 (4) (1979) 381–392.

[61] S. Krause, A. Bronstert, E. Zehe, Groundwater-surface water interactions in a North German lowland floodplain–implications for the river discharge dynamics and riparian water balance, Journal of Hydrology 347 (3) (2007) 404–417.

[62] M. A. Briggs, L. K. Lautz, J. M. McKenzie, R. P. Gordon, D. K. Hare, Using high-resolution distributed temperature sensing to quantify spatial and temporal variability in vertical hyporheic flux, Water Resources Research 48 (2) (2012) W02527.

[63] H. Haitjema, On the residence time distribution in idealized groundwatersheds, Journal of Hydrology 172 (1) (1995) 127–146.